SURFACE OF REVOLUTION RADON TRANSFORMS WITH CENTERS ON GENERALIZED SURFACES IN $\mathbb{R}^n$

27/12/2023 03:16

JAMES W. WEBBER†, SEAN HOLMAN‡, AND ERIC TODD QUINTO*

Abstract. We present a novel analysis of a Radon transform, R, which maps an L^2 function of compact support to its integrals over smooth surfaces of revolution with centers on an embedded hypersurface in $\mathbb{R}^n$. Using microlocal analysis, we derive necessary and sufficient conditions relating to R for the Bolker condition to hold, which has implications regarding the existence and location of image artifacts. We present a general inversion framework based on Volterra equation theory and known results on the spherical Radon transform, and we prove injectivity results for R. Several example applications of our theory are discussed in the context of, e.g., Compton Scatter Tomography (CST) and Ultrasound Reflection Tomography (URT). In addition, using the proposed inversion framework, we validate our microlocal theory via simulation, and present simulated image reconstructions of image phantoms with added noise.

Keywords - surfaces of revolution, generalized Radon transforms, inversion methods, microlocal analysis

1. Introduction

In this paper, we analyze a novel generalized Radon transform, R, which gives the integrals of a compactly supported L^2 function over surfaces of revolution with centers on a smooth hypersurface in $\mathbb{R}^n$. We investigate the inversion stability of R using microlocal analysis, and show that R is injective using known theory on the spherical Radon transform.

There is now a wealth of literature covering the inversion and stability properties of surface of revolution Radon transforms [2, 14, 23, 9, 33, 26, 3, 24, 16, 29, 6, 31, 20, 22, 21, 4, 34, 32, 7], which have applications in, e.g., CST [22], Emission CST (ECST) [29], seismic imaging [7], Synthetic Aperture Radar (SAR) [26], and URT [31].

In [34], the authors consider the microlocal properties of a Radon transform, denoted R (using the notation of [34]), which defines the integrals of an L^2 function over the surfaces of revolution of continuous curves defined by a function, q. The surfaces of revolution considered have centers on a flat plane, and the axes of revolution are perpendicular to the plane of centers. In this case, R is shown to be an elliptic Fourier Integral Operator (FIO) under certain conditions on q. Further, the authors provide necessary and sufficient conditions on q for R to satisfy the Bolker condition, which has important implications regarding image artifacts. Simulated image reconstructions are shown to verify

(James W. Webber (corresponding author)) Department of Oncology and Gynecology, Brigham and Women's Hospital, 221 Longwood Ave., Boston, MA 02115

(Sean Holman) Department of Mathematics, The University of Manchester, Alan Turing Building, Oxford Road, Manchester M13 9PY

(Eric Todd Quinto) Department of Mathematics, Tufts University, 177 College Ave, Medford, MA 02155

E-mail addresses: jwebber5@bwh.harvard.edu†, sean.holman@manchester.ac.uk‡, todd.quinto@tufts.edu*.

the microlocal theory in specific examples where the Bolker condition does, and does not hold.

In [22], the authors present contour reconstruction methods for FIO which define the integrals of a function over lemons, i.e., the surfaces of revolution of circular arcs. A lemon surface has two points of self-intersection. In the geometry of [22], one of the points of self-intersection of the lemon is fixed on the surface of a sphere, and the other moves around on the same sphere. Using microlocal analysis and filtered backprojection ideas, the authors show that the image contours can be recovered from lemon integral data. Simulated image reconstructions of image phantoms are presented with varying levels of added noise, and Total Variation (TV) denoising is applied to help combat noise.

In [27], the author derives inversion formulae for a cone Radon transform, C^k, in n dimensions, and investigates the microlocal properties of C^k. The cones considered have fixed central axis direction. All cones opening angles and vertex positions are used. The authors prove that C^k and its dual are FIOs, and show that the normal operator of C^k is pseudodifferential operator, which has important implication regarding the stability of inversion of C^k. The range of C^k is also explored, and the authors present a differential equation which C^k satisfies, which takes steps towards characterizing the range of C^k. The same author also provides explicit reconstruction formulae for cone transforms with cone points in fairly general positions in [28].

In [14], the authors present explicit inversion formulae for a Radon transform which is defined by the integrals of an n-dimensional function over $(n-1)$-dimensional spheres with centers on the boundary of a closed ball, B, which has radius R, center zero. The target function, f, is assumed to be supported on B. The derivation uses certain properties of the Helmholtz equation in $\mathbb{R}^n$, and an integral representation for f which involves a convolution of f with a solution to the Helmholtz equation. This leads to an inversion formula of filtered backprojection type. Using the proposed inversion formulae, the authors present simulated reconstructions of characteristic functions in two and three-dimensions with added noise.

In this paper, we present a novel inversion framework and microlocal analyses for a new Radon transform, R, which is defined by the integrals of a compactly supported L^2 function, f, over surfaces of revolution with centers on a hypersurface in $\mathbb{R}^n$. This work has important application in, e.g., CST, ECST, and URT. The surfaces of integration we consider are the surfaces of revolution of smooth curves, which are defined by a function, h. The surface of centers we consider is of the form $S = Q \times \mathbb{R} \subset \mathbb{R}^n$, where $Q \subset \mathbb{R}^{n-1}$ is an $(n-2)$-dimensional embedded hypersurface. S can be thought of as a generalized cylinder in the sense that in the special case when $Q = S^{n-2}$ (i.e., when Q is a sphere, dimension $n-2$), S defines a cylinder in $\mathbb{R}^n$. Such center surfaces have been considered previously in [9], where the authors provide explicit inversion formulae for a spherical Radon transform. Using microlocal analysis, we provide necessary and sufficient conditions on S and h for R to be a nondegenerate FIO which satisfies the Bolker condition. This has important implications regarding the existence of image artifacts. Using a combination of Volterra integral equation theory [30] and known results on the spherical Radon transform [20], we prove injectivity results for R, and provide a novel inversion framework to recover f from Rf data. Specific cases of this theory have been considered previously in, e.g., [32, 31]. The results of [32, sections 3 and 4] are a special case of our theory when S is a cylinder in $\mathbb{R}^3$ and h defines a circular arc, and thus the work presented here is a direct generalization of the theory of [32]. In [31], the authors present microlocal analyses of ellipsoid and hyperboloid Radon transforms, and they provide conditions for the Bolker condition to be satisfied. The surfaces of revolution we consider are more general than

ellipsoids and hyperboloids of revolution, and thus the microlocal theory we present here is not covered by [31].

In [34], surface of revolution transforms are also considered, and the authors derive conditions which are equivalent to the Bolker condition. In [34], the integral surface centers are constrained to a flat plane, and the surfaces of revolution have central axes which are perpendicular to the plane of centers. In this work, we consider more general center surfaces than a flat plane (i.e., the S as described above), and the surfaces of revolution we consider have axes of revolution which are embedded in S. Thus, the theory of [34] does not apply to this work.

The surface of centers we consider (S) bears similarities with that of [9]. In [9], only spherical integral surfaces are considered. We consider much more general integrals surfaces, which are the surfaces of revolution of smooth curves defined by a function, h. Spherical integral surfaces are a special case of our theory, when h is set to define a semicircular curve.

In addition to the microlocal and injectivity theory presented, we also discuss multiple applications of our theory, e.g., in CST, ECST, and URT, and, using the proposed inversion method, we present simulated image reconstructions in the context of CST and URT.

The remainder of this paper is organized as follows. In section 2, we state some preliminary definitions and theory from microlocal analysis that we apply later to prove our theorems. In section 3, we introduce a new Radon transform, R, and prove our first main theorem which gives conditions for R to be an FIO which satisfies the Bolker condition. In section 4 we prove injectivity results for R and present an inversion framework. In section 5, we discuss some example applications of our theory to CST, ECST, and URT. To finish, we present simulated image reconstructions in section 6 to validate our microlocal theory, and we present reconstructions of image phantoms with added noise.

2. Definitions

In this section, we review some theory from microlocal analysis which will be used in our theorems. We first provide some notation and definitions. Let X and Y be open subsets of $\mathbb{R}^{n_X}$ and $\mathbb{R}^{n_Y}$, respectively. Let $\mathcal{D}(X)$ be the space of smooth functions compactly supported on X with the standard topology and let $\mathcal{D}'(X)$ denote its dual space, the vector space of distributions on X. Let $\mathcal{E}(X)$ be the space of all smooth functions on X with the standard topology and let $\mathcal{E}'(X)$ denote its dual space, the vector space of distributions with compact support contained in X. Finally, let $\mathcal{S}(\mathbb{R}^n)$ be the space of Schwartz functions, that are rapidly decreasing at ∞ along with all derivatives. See [25] for more information.

If $A \subset \mathbb{R}^n$, then $\text{int}(A)$ and $\text{bd}(A)$ are, respectively, the interior of A and the boundary of A.

We now list some notation conventions that will be used throughout this paper:

(1) For a function f in the Schwartz space $\mathcal{S}(\mathbb{R}^{n_X})$ or in $L^2(\mathbb{R}^{n_X})$, we use $\mathcal{F}f$ and $\mathcal{F}^{-1}f$ to denote the Fourier transform and inverse Fourier transform of f, respectively (see [11, Definition 7.1.1]).

(2) We use the standard multi-index notation: if $\alpha = (\alpha_1, \alpha_2, \ldots, \alpha_n) \in \{0, 1, 2, \ldots\}^{n_X}$ is a multi-index and f is a function on $\mathbb{R}^{n_X}$, then

$$\partial^\alpha f = \left(\frac{\partial}{\partial x_1}\right)^{\alpha_1} \left(\frac{\partial}{\partial x_2}\right)^{\alpha_2} \cdots \left(\frac{\partial}{\partial x_{n_X}}\right)^{\alpha_{n_X}} f.$$

If f is a function of $(\mathbf{y}, \mathbf{x}, \boldsymbol{\sigma})$ then $\partial^\alpha_{\mathbf{y}} f$ and $\partial^\alpha_{\boldsymbol{\sigma}} f$ are defined similarly.

(3) We identify the cotangent spaces of Euclidean spaces with the underlying Euclidean spaces. For example, the cotangent space, $T^*(X)$, of X is identified with $X \times \mathbb{R}^{n_X}$. If Φ is a function of $(\mathbf{y}, \mathbf{x}, \boldsymbol{\sigma}) \in Y \times X \times \mathbb{R}^N$, then we define $\mathrm{d}_{\mathbf{y}}\Phi = \left(\frac{\partial \Phi}{\partial y_1}, \frac{\partial \Phi}{\partial y_2}, \cdots, \frac{\partial \Phi}{\partial y_{n_X}}\right)$, and $\mathrm{d}_{\mathbf{x}}\Phi$ and $\mathrm{d}_{\boldsymbol{\sigma}}\Phi$ are defined similarly. Identifying the cotangent space with the Euclidean space as mentioned above, we let $\mathrm{d}\Phi = (\mathrm{d}_{\mathbf{y}}\Phi, \mathrm{d}_{\mathbf{x}}\Phi, \mathrm{d}_{\boldsymbol{\sigma}}\Phi)$.

(4) For $\Omega \subset \mathbb{R}^m$, we define $\dot{\Omega} = \Omega \setminus \mathbf{0}$.

The singularities of a function and the directions in which they occur are described by the wavefront set [5, page 16], which we now define.

Definition 2.1. Let X be an open subset of $\mathbb{R}^{n_X}$ and let f be a distribution in $\mathcal{D}'(X)$. Let $(\mathbf{x}_0, \boldsymbol{\xi}_0) \in X \times \dot{\mathbb{R}^n}$. Then f is *smooth at* $\mathbf{x}_0$ *in direction* $\boldsymbol{\xi}_0$ if there exists a neighborhood U of $\mathbf{x}_0$ and V of $\boldsymbol{\xi}_0$ such that for every $\Phi \in \mathcal{D}(U)$ and $N \in \mathbb{R}$ there exists a constant C_N such that for all $\boldsymbol{\xi} \in V$,

$$|\mathcal{F}(\Phi f)(\lambda \boldsymbol{\xi})| \leq C_N (1 + |\lambda|)^{-N}. \tag{2.1}$$

The pair $(\mathbf{x}_0, \boldsymbol{\xi}_0)$ is in the *wavefront set,* $\mathrm{WF}(f)$, if f is not smooth at $\mathbf{x}_0$ in direction $\boldsymbol{\xi}_0$.

Intuitively, the elements $(\mathbf{x}_0, \boldsymbol{\xi}_0) \in \mathrm{WF}(f)$ are the point-normal vector pairs at which f has singularities; $\mathbf{x}_0$ is the location of the singularity, and $\boldsymbol{\xi}_0$ is the direction in which the singularity occurs. A geometric example of the wavefront set is given by the characteristic function f of a domain $\Omega \subset \mathbb{R}^{n_X}$ with smooth boundary, which is 1 on Ω and 0 off of Ω. Then the wavefront set is

$$\mathrm{WF}(f) = \{(\mathbf{x}, t\mathbf{v}) \ : t \neq 0, \ \mathbf{x} \in \partial\Omega, \ \mathbf{v} \text{ is orthogonal ot } \partial\Omega \text{ at } \mathbf{x}\}.$$

In other words, the wavefront set is the set of points in the boundary of Ω together with the nonzero normal vectors to the boundary. The wavefront set is an important consideration in imaging since elements of the wavefront set will correspond to sharp features of an image.

The wavefront set of a distribution on X is normally defined as a subset the cotangent bundle $T^*(X)$ so it is invariant under diffeomorphisms, but we do not need this invariance, so we will continue to identify $T^*(X) = X \times \mathbb{R}^{n_X}$ and consider $\mathrm{WF}(f)$ as a subset of $X \times \dot{\mathbb{R}^{n_X}}$.

Definition 2.2 ([11, Definition 7.8.1])**.** We define $S^m(Y \times X, \mathbb{R}^N)$ to be the set of $a \in \mathcal{E}(Y \times X \times \mathbb{R}^N)$ such that for every compact set $K \subset Y \times X$ and all multi–indices α, β, γ the bound

$$\left|\partial_{\mathbf{y}}^{\gamma} \partial_{\mathbf{x}}^{\beta} \partial_{\boldsymbol{\sigma}}^{\alpha} a(\mathbf{y}, \mathbf{x}, \boldsymbol{\sigma})\right| \leq C_{K,\alpha,\beta,\gamma} (1 + \|\boldsymbol{\sigma}\|)^{m - |\alpha|}, \quad (\mathbf{y}, \mathbf{x}) \in K, \ \boldsymbol{\sigma} \in \mathbb{R}^N,$$

holds for some constant $C_{K,\alpha,\beta,\gamma} > 0$.

The elements of S^m are called *symbols* of order m. Note that this symbol class is sometimes denoted $S^m_{1,0}$. The symbol $a \in S^m(Y \times X, \mathbb{R}^N)$ is *elliptic* if for each compact set $K \subset Y \times X$, there is a $C_K > 0$ and $M > 0$ such that

$$|a(\mathbf{y}, \mathbf{x}, \boldsymbol{\sigma})| \geq C_K (1 + \|\boldsymbol{\sigma}\|)^m, \quad (\mathbf{y}, \mathbf{x}) \in K, \ \|\boldsymbol{\sigma}\| \geq M. \tag{2.2}$$

Definition 2.3 ([12, Definition 21.2.15])**.** A function $\Phi = \Phi(\mathbf{y}, \mathbf{x}, \boldsymbol{\sigma}) \in \mathcal{E}(Y \times X \times \dot{\mathbb{R}^N})$ is a *phase function* if $\Phi(\mathbf{y}, \mathbf{x}, \lambda\boldsymbol{\sigma}) = \lambda\Phi(\mathbf{y}, \mathbf{x}, \boldsymbol{\sigma})$, $\forall \lambda > 0$ and $\mathrm{d}\Phi$ is nowhere zero. The *critical set of* Φ is

$$\Sigma_\Phi = \{(\mathbf{y}, \mathbf{x}, \boldsymbol{\sigma}) \in Y \times X \times \dot{\mathbb{R}^N} : \mathrm{d}_{\boldsymbol{\sigma}}\Phi = 0\}.$$

A phase function is *clean* if the critical set $\Sigma_\Phi = \{(\mathbf{y}, \mathbf{x}, \boldsymbol{\sigma}) \ : \ \mathrm{d}_{\boldsymbol{\sigma}}\Phi(\mathbf{y}, \mathbf{x}, \boldsymbol{\sigma}) = 0\}$ is a smooth manifold with tangent space defined by the kernel of $\mathrm{d}\left(\mathrm{d}_\sigma\Phi\right)$ on Σ_Φ. Here, the derivative d is applied component-wise to the vector-valued function $\mathrm{d}_\sigma\Phi$. So, $\mathrm{d}\left(\mathrm{d}_\sigma\Phi\right)$ is treated as a Jacobian matrix of dimensions $N \times (2n + N)$.

By the Constant Rank Theorem the requirement for a phase function to be clean is satisfied if $\mathrm{d}\left(\mathrm{d}_{\boldsymbol{\sigma}}\Phi\right)$ has constant rank.

Definition 2.4 ([12, Definition 21.2.15] and [13, section 25.2])**.** Let X and Y be open subsets of $\mathbb{R}^n$. Let $\Phi \in \mathcal{E}\left(Y \times X \times \mathbb{R}^N\right)$ be a clean phase function. In addition, we assume that Φ is *nondegenerate* in the following sense:

$$\mathrm{d}_{\mathbf{y}}\Phi \text{ and } \mathrm{d}_{\mathbf{x}}\Phi \text{ are never zero on } \Sigma_\Phi.$$

The *canonical relation parametrized by* Φ is defined as

$$\mathcal{C} = \{((\mathbf{y}, \mathrm{d}_{\mathbf{y}}\Phi(\mathbf{y}, \mathbf{x}, \boldsymbol{\sigma}))\,; (\mathbf{x}, -\mathrm{d}_{\mathbf{x}}\Phi(\mathbf{y}, \mathbf{x}, \boldsymbol{\sigma}))) : (\mathbf{y}, \mathbf{x}, \boldsymbol{\sigma}) \in \Sigma_\Phi\}\,, \tag{2.3}$$

Definition 2.5. Let X and Y be open subsets of $\mathbb{R}^{n_X}$ and $\mathbb{R}^{n_Y}$, respectively. Let an operator $A : \mathcal{D}(X) \to \mathcal{D}'(Y)$ be defined by the distribution kernel $K_A \in \mathcal{D}'(Y \times X)$, in the sense that $Af(\mathbf{y}) = \int_X K_A(\mathbf{y}, \mathbf{x}) f(\mathbf{x}) \mathrm{d}\mathbf{x}$. Then we call K_A the *Schwartz kernel* of A. A *Fourier integral operator (FIO)* of order $m + N/2 - (n_X + n_Y)/4$ is an operator $A : \mathcal{D}(X) \to \mathcal{D}'(Y)$ with Schwartz kernel given by an oscillatory integral of the form

$$K_A(\mathbf{y}, \mathbf{x}) = \int_{\mathbb{R}^N} e^{i\Phi(\mathbf{y}, \mathbf{x}, \boldsymbol{\sigma})} a(\mathbf{y}, \mathbf{x}, \boldsymbol{\sigma}) \mathrm{d}\boldsymbol{\sigma}, \tag{2.4}$$

where Φ is a clean nondegenerate phase function and a is a symbol in $S^m(Y \times X, \mathbb{R}^N)$. The *canonical relation of* A is the canonical relation of Φ defined in (2.3). A is called an *elliptic* FIO if its symbol is elliptic. An FIO is called a *pseudodifferential operator* if its canonical relation $\mathcal{C}$ is contained in the diagonal, i.e., $\mathcal{C} \subset \Delta := \{(\mathbf{x}, \boldsymbol{\xi}; \mathbf{x}, \boldsymbol{\xi})\}$.

Formula (2.4) given in Definition 2.5 can be extended to operators which are only locally represented by kernels in the form (2.4) as in [13], although we will not require this in the present manuscript. We also note that pseudodifferential operators can always be defined by (2.4) with phase function $\Phi(\mathbf{y}, \mathbf{x}, \boldsymbol{\sigma}) = (\mathbf{y} - \mathbf{x}) \cdot \boldsymbol{\sigma}$.

Let X and Y be sets and let $\Omega_1 \subset X$ and $\Omega_2 \subset Y \times X$. The composition $\Omega_2 \circ \Omega_1$ and transpose Ω_2^t of Ω_2 are defined

$$\Omega_2 \circ \Omega_1 = \{\mathbf{y} \in Y : \exists \mathbf{x} \in \Omega_1,\ (\mathbf{y}, \mathbf{x}) \in \Omega_2\}$$
$$\Omega_2^t = \{(\mathbf{x}, \mathbf{y}) : (\mathbf{y}, \mathbf{x}) \in \Omega_2\}\,.$$

We now state the Hörmander-Sato Lemma [11, Theorem 8.2.13], which provides the relationship between the wavefront set of distributions and their images under FIO.

Theorem 2.6 (Hörmander-Sato Lemma)**.** *Let $f \in \mathcal{E}'(X)$ and let $A : \mathcal{E}'(X) \to \mathcal{D}'(Y)$ be an FIO with canonical relation $\mathcal{C}$. Then,* $\mathrm{WF}(Af) \subset \mathcal{C} \circ \mathrm{WF}(f)$.

Let A be an FIO, then its formal adjoint A^* is also an FIO, and if $\mathcal{C}$ is the canonical relation of A, then the canonical relation of A^* is $\mathcal{C}^t$ [10]. Many imaging techniques are based on application of the adjoint operator A^* and so to understand artifacts we consider A^*A (or, if A does not map to $\mathcal{E}'(Y)$, then $A^*\psi A$ for an appropriate cutoff ψ). Because of Theorem 2.6,

$$\mathrm{WF}(A^*\psi Af) \subset \mathcal{C}^t \circ \mathcal{C} \circ \mathrm{WF}(f). \tag{2.5}$$

The next two definitions provide tools to analyze the composition in equation (2.5).

Definition 2.7. Let $\mathcal{C} \subset T^*(Y \times X)$ be the canonical relation associated to the FIO $A : \mathcal{E}'(X) \to \mathcal{D}'(Y)$. We let Π_L and Π_R denote the natural left- and right-projections of $\mathcal{C}$, projecting onto the appropriate coordinates: $\Pi_L : \mathcal{C} \to T^*(Y)$ and $\Pi_R : \mathcal{C} \to T^*(X)$.

Because Φ is nondegenerate, the projections do not map to the zero section. If A satisfies our next definition, then A^*A (or $A^*\psi A$) is a pseudodifferential operator [8, 18].

Definition 2.8 (Bolker condition)**.** Let $A : \mathcal{E}'(X) \to \mathcal{D}'(Y)$ be a FIO with canonical relation $\mathcal{C}$ then A (or $\mathcal{C}$) satisfies the *Bolker Condition* if the natural projection $\Pi_L : \mathcal{C} \to T^*(Y)$ is an embedding (injective immersion).

Thus, using (2.5), we see that under the Bolker condition the wavefront set of $A^*\varphi Af$ will be contained in the wavefront set of f. Intuitively, the reconstructed image $(A^*\varphi Af)$ will only include singularities at the same positions and in the same directions as the original image (f).

3. Surface of revolution transforms

We will consider generalized Radon transforms in Euclidean space of three or more dimensions that integrate over fairly arbitrary collections of surfaces of revolution with axes on a smooth cylindrical surface. For $\mathbf{w} = (w_1, \ldots, w_n) \in \mathbb{R}^n$, we define $\mathbf{w}' = (w_1, \ldots, w_{n-1}) \in \mathbb{R}^{n-1}$ throughout this paper. The generalized cylindrical surface in $\mathbb{R}^n$ is defined by a smooth embedded hypersurface $Q \subset \mathbb{R}^{n-1}$ and with axis parallel the x_n axis:

$$S = Q \times \mathbb{R}. \tag{3.1}$$

Each $\mathbf{y} \in S$ is on a unique line $\ell_{\mathbf{y}}$ contained in S and parallel the x_n axis. Our surfaces of revolution will be determined by specifying the distance from $\ell_{\mathbf{y}}$ to each point on the surface. Let $h = h(s, x)$ be a nonnegative smooth function from Ω_h to $\mathbb{R}$, where $\Omega_h \subset \mathbb{R}^2$ is open, let $C = \{s \in \mathbb{R} : \exists x \in \mathbb{R} \text{ s.t. } (s, x) \in \Omega_h\}$, and let

$$Y = C \times S.$$

Our surfaces are defined as follows. Let $(s, \mathbf{y}) \in Y$ and define

$$\begin{aligned} \Psi(s, \mathbf{y}; \mathbf{x}) &= (\mathbf{x}' - \mathbf{y}') \cdot (\mathbf{x}' - \mathbf{y}') - h(s, x_n - y_n) \\ \mathcal{R}(s, \mathbf{y}) &= \{\mathbf{x} \in \mathbb{R}^n : \Psi(s, \mathbf{y}; \mathbf{x}) = 0\}. \end{aligned} \tag{3.2}$$

When $(s, \mathbf{y}) \in Y$, $\mathcal{R}(s, \mathbf{y})$ is the surface of revolution about $\ell_{\mathbf{y}}$ of the smooth curve defined by $x_n \mapsto \sqrt{h}(s, x_n - y_n)$. Varying s changes the curve defining the surface of revolution. If one fixes $s \in C$ and $\mathbf{y}' \in Q$, then the surfaces $\mathcal{R}(s, (\mathbf{y}', y_n))$ are translates of each other along $\ell_{\mathbf{y}}$ as y_n varies. An example S, $\mathcal{R}(s, \mathbf{y})$, and $\sqrt{h}$ curve are illustrated in figure 1, in $n = 3$ dimensions. Now we define our Radon transform.

Definition 3.1. Let D be an open set disjoint from S. Let $f \in \mathcal{D}(D)$ and $(s, \mathbf{y}) \in Y$. Our Radon transform $Rf(s, \mathbf{y})$ is defined to be the integral of f over $\mathcal{R}(s, \mathbf{y})$ in surface area measure:

$$Rf(s, \mathbf{y}) = \int_{\mathbb{R}^n} |\nabla_{\mathbf{x}} \Psi(s, \mathbf{y}; \mathbf{x})| \delta(\Psi(s, \mathbf{y}; \mathbf{x})) f(\mathbf{x}) \, \mathrm{d}\mathbf{x}. \tag{3.3}$$

It is also possible to extend R to $\mathcal{E}'(D)$ by continuity.

In our results, we will put conditions on h so that $\mathcal{R}(s, \mathbf{y})$ is a smooth embedded manifold. We can now state the main theorem of this section.

Theorem 3.2. *Let Q be an embedded smooth hypersurface in $\mathbb{R}^{n-1}$ and let $S = Q \times \mathbb{R}$. Let D be an open set in $\mathbb{R}^n$, which is disjoint from S.*

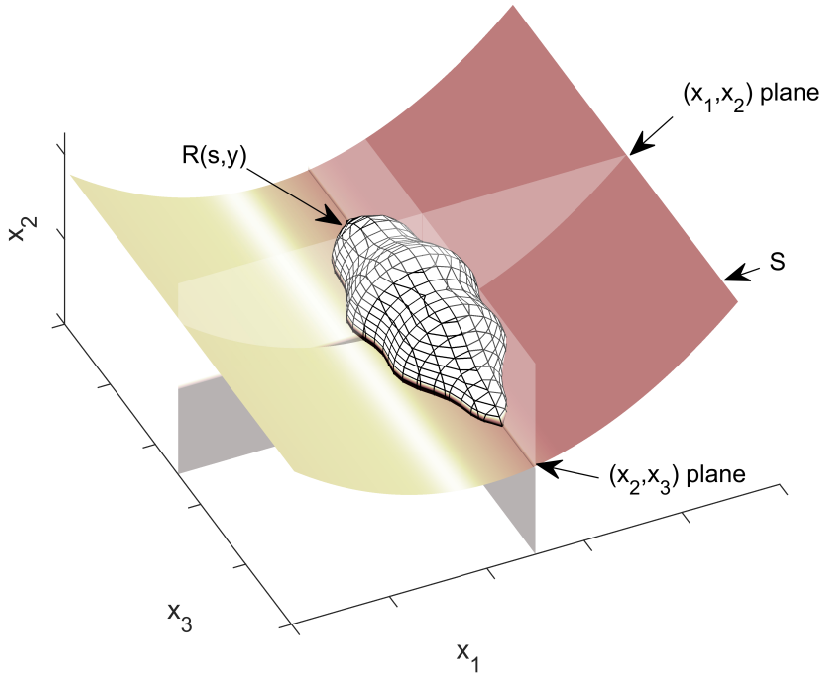

(A) 3-D view

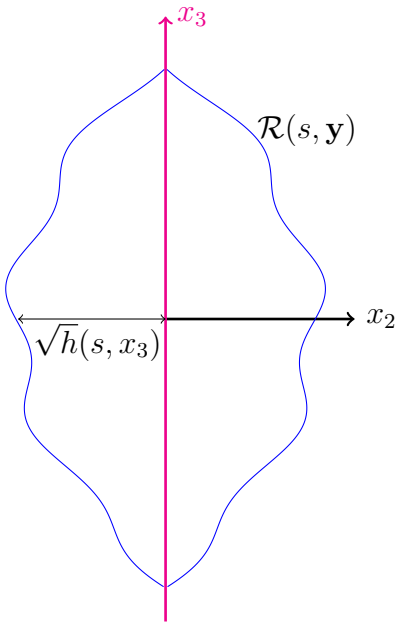

(B) (x_2, x_3) plane

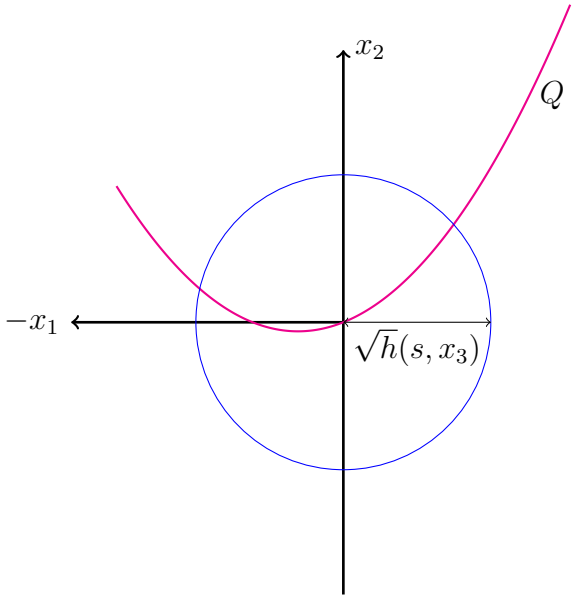

(C) (x_1, x_2) plane

FIGURE 1. Example S and $\mathcal{R}(s, \mathbf{y})$ when $n = 3$. (A) - 3-D view. (B) - (x_2, x_3) plane cross-section. (C) - (x_1, x_2) plane cross-section. The plane slices in (B) and (C) are labeled in (A). The pink smooth surface in (A) is S, and the black and white meshed surface in (A) is $\mathcal{R}(s, \mathbf{y})$. The pink line in (B) is a line, $\ell_{\mathbf{y}}$ ($\mathbf{y} = 0$ in this example), as described in the main text. The pink curve in (C), is Q. The blue curves in (B) and (C) (e.g., the circle in (C)) are the intersections of $\mathcal{R}(s, \mathbf{y})$ with the (x_2, x_3) and (x_1, x_2) planes, respectively. The blue wavy curve in (B) is $\{(\pm\sqrt{h}(s, x_3), x_3)\}$.

(1) For each $s \in C$, let

$$\Omega_{h,s} = \{x \in \mathbb{R} : (s,x) \in \Omega_h\},$$

and assume, for each $s \in C$, that $h(s,\cdot) \to 0$ on the boundary of $\Omega_{h,s}$.

(2) Let $(s,\mathbf{y}) \in Y$ and $\mathbf{x}$ be any point in $D \cap \mathcal{R}(s,\mathbf{y})$. Assume that the reflection of $\mathbf{x}$ in the tangent plane, T, to S at $\mathbf{y}$ is not in D.

(3) Assume for every $(s,x) \in \Omega_h$, $h_s(s,x) \neq 0$.

(4) Assume for each fixed $s \in C$, the function $(h_x/h_s)(s,\cdot)$ is injective on $\{x \in \mathbb{R} : (s,x) \in \Omega_h\}$.

(5) Assume $\frac{\mathrm{d}}{\mathrm{d}x}(h_x/h_s) \neq 0$ on Ω_h.

Then $R : \mathcal{E}'(D) \to \mathcal{D}'(Y)$ is a nondegenerate FIO that satisfies the Bolker condition.

Conversely, assume R satisfies the Bolker assumption above D, and h satisfies (3)*. Then* (2)*,* (4)*, and* (5) *all hold.*

Note that assumption (1) holds if $h \to 0$ on $\mathrm{bd}(\Omega_h)$, but this more general version will be useful for the example in section 5.2. Regarding assumption (2), if $\mathbf{x} \in D \cap \mathcal{R}(s,\mathbf{y})$ and its reflection $\mathbf{x}_m$ in a tangent plane T to S at $\mathbf{y}$ is also in D, then Π_L will not be injective and reconstructions using the normal operator can create artifacts at $\mathbf{x}_m$ from singularities at $\mathbf{x}$. Condition (2) would be valid if D is connected, open and disjoint from every tangent plane to S. A common special case occurs when S is a smooth surface that is the boundary of a convex cylinder; then (2) holds if D is inside the convex cylinder. If $\mathbf{x} \in T$, then $\mathbf{x}$ is its own mirror point. Therefore, we will interpret (2) to mean that $D \cap \mathcal{R}(s,\mathbf{y})$ is disjoint from T.

Example 3.3. Here are two interesting transforms in $\mathbb{R}^3$ that fit in our theory. More general algebraic surfaces were considered in [31]. Let Q be a smooth hypersurface in $\mathbb{R}^2$ and let $S = Q \times \mathbb{R}$ and let $Y = (0,\infty) \times S$.

The spherical transform: Let $h(s,x) = s - x^2$. Then $\mathcal{R}(s,\mathbf{y})$ is the sphere $(x_1-y_1)^2 + (x_2-y_2)^2 + (x_3-y_3)^2 = s$ for $(s,\mathbf{y}) \in Y$.

The transform on hyperboloids of two sheets: Let $h(s,x) = x^2 + s$. Then $\mathcal{R}(s,\mathbf{y})$ is the hyperboloid of two sheets with axis of rotation $\{\mathbf{y}'\} \times \mathbb{R}$ and equation $(x_1-y_1)^2 + (x_2-y_2)^2 - (x_3-y_3)^2 = s$ for $(s,\mathbf{y}) \in Y$.

Proof. Because the Bolker condition is local above Y, we will define Q locally as a graph using coordinates. For convenience, we now define $\mathbf{y}'' = (y_2,\ldots,y_{n-1}) \in \mathbb{R}^{n-2}$. Let Ω be an open set in $\mathbb{R}^{n-2}$, the domain of the coordinates, and suppose Q is the graph of a function $q \in C^\infty(\Omega,\mathbb{R})$. That is,

$$Q = \{(q(\mathbf{y}''),\mathbf{y}'') : \mathbf{y}'' \in \Omega\}, \qquad S = Q \times \mathbb{R}$$

and

$$(\mathbf{y}'', y_n) \mapsto (q(\mathbf{y}''),\mathbf{y}'', y_n)$$

give coordinates on S. Using these coordinates, our Radon transform can be written

$$\begin{aligned} Rf(s,(\mathbf{y}'',y_n)) &= \int_{\mathbb{R}^n} |\nabla_{\mathbf{x}}\Psi| \delta\left(\Psi(s,(\mathbf{y}'',y_n);\mathbf{x})\right) f(\mathbf{x}) \mathrm{d}\mathbf{x} \\ &= \int_{-\infty}^{\infty} \int_{\mathbb{R}^n} |\nabla_{\mathbf{x}}\Psi| f(\mathbf{x}) e^{i\sigma\Psi(s,(\mathbf{y}'',y_n);\mathbf{x})} \mathrm{d}\mathbf{x}\mathrm{d}\sigma, \end{aligned} \tag{3.4}$$

where

$$\Psi(s,(\mathbf{y}'',y_n);\mathbf{x}) = (x_1 - q(\mathbf{y}''))^2 + (\mathbf{x}'' - \mathbf{y}'') \cdot (\mathbf{x}'' - \mathbf{y}'') - h(s, x_n - y_n).$$

Note, the integral in (3.4) is well-defined given that, by assumption, D is bounded away from S, and h goes to zero at the boundary of Ω_h. Then, the phase function of R is $\Phi = \sigma\Psi$. The weight, $|\nabla_{\mathbf{x}}\Psi|$, is included following the theory of [17], so that the integrals are defined with respect to the surface measure on the surfaces of revolution.

We now explain why Φ is a nondegenerate phase function. From (3.5) just below and assumption (3) in our theorem, one sees $\mathrm{d}_s\Phi$ is never zero so the left projection is never zero. A calculation shows that

$$\mathrm{d}_{\mathbf{x}}\Phi = \sigma\left(2[(x_1, \mathbf{x}'') - (q, \mathbf{y}'')], -h_x(s, x_n - y_n)\right),$$

and this is never zero since D is disjoint from the cylinder S. In addition, this shows $\mathcal{R}(s, (\mathbf{y}'', y_n)) \cap D$ is a smooth manifold, so R is a standard Radon transform.

The left projection of R is

$$\Pi_L(s, (\mathbf{y}'', y_n); \mathbf{x}, \sigma) = \left(s, (\mathbf{y}'', y_n), \overbrace{-\sigma h_s}^{\mathrm{d}_s\Phi}, \overbrace{-2\sigma\left[(x_1 - q)\nabla q + (\mathbf{x}'' - \mathbf{y}'')\right]}^{\mathrm{d}_{\mathbf{y}''}\Phi}, \overbrace{\sigma h_x}^{\mathrm{d}_{y_n}\Phi}\right), \tag{3.5}$$

where $\nabla q = (q_2, \ldots, q_{n-2})^T$, and we use the convention $q_i = q_{y_i}$.

Let

$$\Pi_L(s, (\mathbf{y}'', y_n), (\mathbf{x}^{(1)\prime}, x_n^{(1)}), \sigma_1) = \Pi_L(s, (\mathbf{y}'', y_n), (\mathbf{x}^{(2)\prime}, x_n^{(2)}), \sigma_2). \tag{3.6}$$

Using (3) and that the $\mathrm{d}_s\Phi$ and the $\mathrm{d}_{y_n}\Phi$ components in (3.5)are equal, we see

$$\frac{h_x}{h_s}\left(s, x_n^{(1)} - y_n\right) = \frac{h_x}{h_s}\left(s, x_n^{(2)} - y_n\right) \implies x_n = x_n^{(1)} = x_n^{(2)}, \tag{3.7}$$

by condition (4). Further $\sigma_1 = \sigma_2$ since $h_s \neq 0$ by condition (3).

Setting the $\mathrm{d}_{\mathbf{y}''}$ components of Π_L equal, we see

$$[\nabla q, I]\left(\mathbf{x}^{(1)\prime} - \mathbf{x}^{(2)\prime}\right) = 0. \tag{3.8}$$

The rows of $A = [\nabla q, I]$ span a plane parallel to the plane tangent to Q at $(q, \mathbf{y}''))$, and

$$\mathrm{null}(A) = \{\nu(1, -\nabla q)^T : \nu \in \mathbb{R}\}.$$

Thus, $\mathbf{x}^{(1)\prime}$ and $\mathbf{x}^{(2)\prime}$ must lie on a line parallel to $(1, -\nabla q)^T$. As $\mathbf{x}^{(1)\prime}$ and $\mathbf{x}^{(2)\prime}$ are also on the same sphere centered at $(q, \mathbf{y}'')$ of radius $h(s, x_n - y_n)$, either $\mathbf{x}^{(1)\prime}$ and $\mathbf{x}^{(2)\prime}$ are equal or they are the reflections of one another in the tangent plane to Q at $(q, \mathbf{y}'')$. Thus, $\mathbf{x}_1$ and $\mathbf{x}_2$ are either equal or the reflections of one another in the plane tangent to S at $(\mathbf{y}'', y_n)$. By our assumption (2), $\mathbf{x}^{(1)\prime} = \mathbf{x}^{(2)\prime}$ and Π_L is injective above D.

For $\mathbf{x} \in \mathcal{R}(s, (\mathbf{y}'', y_n))$, $(x_1, \mathbf{x}'')$ lies on an $n-2$ dimensional sphere of radius $\sqrt{h}(s, x_n - y_n)$. Let us parameterize this sphere using standard spherical coordinates $\alpha = (\alpha_1, \ldots, \alpha_{n-2})$. Then,

$$(x_1, \mathbf{x}'') = (q(\mathbf{y}''), \mathbf{y}'') + \sqrt{h}(s, x_n - y_n)\Theta(\alpha) = (q, \mathbf{y}'') + \sqrt{h}\Theta, \tag{3.9}$$

where $\Theta = \Theta(\alpha) \in S^{n-2}$ is not a pole of the sphere. Now, equation (3.5) becomes

$$\Pi_L(s, (\mathbf{y}'', y_n), \alpha, x_n, \sigma) = \left(s, (\mathbf{y}'', y_n), \overbrace{-\sigma h_s}^{\mathrm{d}_s\Phi}, \overbrace{-2\sigma\sqrt{h}\left[\nabla q, I\right]\Theta^T}^{\mathrm{d}_{\mathbf{y}''}}, \overbrace{\sigma h_x}^{\mathrm{d}_{y_n}\Phi}\right), \tag{3.10}$$

where $I = I_{(n-2)\times(n-2)}$. Since $h > 0$ on $\mathcal{R}(s, (\mathbf{y}'', y_n))$, these coordinates are smooth.

The differential of Π_L is

$$D\Pi_L = \begin{array}{c} \\ s,(\mathbf{y}'',y_n) \\ \mathrm{d}_s\Phi \\ \mathrm{d}_{y_n}\Phi \\ \nabla_{\mathbf{y}''}\Phi \end{array} \begin{array}{c} \begin{array}{cccc} \mathrm{d}s,\nabla_{(\mathbf{y}'',y_n)} & \mathrm{d}\sigma & \mathrm{d}x_n & \nabla_\alpha \end{array} \\ \begin{pmatrix} I_{n\times n} & \mathbf{0}_{n\times 1} & \mathbf{0}_{n\times 1} & \mathbf{0}_{n\times(n-2)} \\ \cdot & -h_s & -\sigma h_{sx_n} & \mathbf{0}_{1\times(n-2)} \\ \cdot & h_x & \sigma h_{xx} & \mathbf{0}_{1\times(n-2)} \\ \cdot & \cdot & \cdot & -2\sigma\sqrt{h}\,[\nabla q, I]\,\Upsilon, \end{pmatrix} \end{array} \tag{3.11}$$

where $\Upsilon = [\Theta^T_{\alpha_1}, \ldots, \Theta^T_{\alpha_{n-2}}]$, and $[\Theta^T, \Upsilon]$ is a matrix with nonzero orthogonal columns.

We have

$$\det\begin{pmatrix} -h_s & -\sigma h_{sx_n} \\ h_x & \sigma h_{xx} \end{pmatrix} = -\sigma\left(h_s h_{xx} - h_x h_{sx_n}\right) = -\sigma h_s^2 \cdot \frac{\mathrm{d}}{\mathrm{d}x_n}\left(\frac{h_x}{h_s}\right) \neq 0, \tag{3.12}$$

by conditions (3) and (5).

If $\det\left([\nabla q, I]\,\Upsilon\right) = 0$, then some linear combination of the columns of Υ is in null(A), so $\nu(1, -\nabla q)^T$ is in the span of the columns of Υ. Since Θ^T is normal to span(Υ), Θ^T must be normal to $(1, -\nabla q)^T$, which means $\mathbf{x}$ is on the plane tangent to S at $(\mathbf{y}'', y_n)$. This is not possible because of (2). Therefore, Π_L is an immersion.

Now, assume R satisfies the Bolker condition above D, and h satisfies (3). Then, R is, by definition, a FIO. Because Π_L is an immersion, Π_R is also an immersion [10], so the phase function Φ is nondegenerate.

Regarding (4), if h_x/h_s is not injective then there are $\sigma_1, \sigma_2, x_n^1, x_n^2$ not all equal to each other such that the third and last components in (3.5) are equal. Since h_s is never zero, this means that equality holds in the left-hand side of (3.7). So, if Bolker holds then (4) is true.

Let $\mathbf{x} \in \mathcal{R}(s, (\mathbf{y}'', y_n))$ and let $\mathbf{x}_m$ be its reflection in the tangent plane, T,to S at $(q, \mathbf{y}'', y_n)$. If $\mathbf{x} \neq \mathbf{x}_m$ and $\mathbf{x}_m \in D$, then the argument around (3.8) shows that Π_L is not injective. This proves (2) for points not on T.

If Bolker holds, the matrix in(3.11), $[\nabla q, I]\Upsilon$, has maximum rank, so span(Υ) contains no nonzero vector in null(A). Therefore, Θ^T in (3.9) is not perpendicular to $(-1, \nabla q)^T$ and $\mathbf{x}$ is not in the tangent plane to S at $(s, (\mathbf{y}'', y_n))$. This shows (2) for points on T. For the same reason, (3.12) must be valid since $h_s \neq 0$. This shows that (5) holds. □

4. An Inversion Framework

We will present two different cases in which inversion of the surface of rotation Radon transform is possible by first taking a Fourier transform in the vertical coordinate.

4.1. **Analytic inversion formula for the cone transform.**

In this section, we consider the case when $h(s, x) = sx$, and $\mathcal{R}(s, \mathbf{y})$ is a cone. In this case, we have the alternate expression for R

$$Rf(s, \mathbf{y}) = \sqrt{1+s^2}\int_0^\infty \int_{\Theta\in S^{n-2}} t^{n-2} f\left(t\Theta + \mathbf{y}', y_n - st\right) \mathrm{d}S^{n-2}\mathrm{d}t, \tag{4.1}$$

where $s \in \mathbb{R}$. Rf defines the integral of f over a cone with gradient s, vertex $\mathbf{y} \in S$, and axis of revolution parallel to x_n which is contained in S.

Next, we will present the theorem which proves injectivity of the cone transform. For the proof we will require the spherical Radon transform

$$M : L_c^2(\mathbb{R}^{n-1}) \to L^2\left(\mathbb{R}_+ \times \mathbb{R}^{n-1}\right)$$

For $f \in L_c^2(\mathbb{R}^{n-1})$, $Mf(t, \mathbf{y}')$ defines the integral of $\hat{f}_\xi \in L_c^2(\mathbb{R}^{n-1})$ over the $(n-2)$-dimensional sphere with radius t and center $\mathbf{y}'$.

Theorem 4.1. *Suppose that $S = Q \times \mathbb{R}$ is a real-analytic manifold and Q is the boundary of an open convex set $\Sigma \subset \mathbb{R}^{n-1}$. Let $f \in L^2_c(\Sigma \times \mathbb{R})$ and $h(s,x) = sx$. Under these conditions, $Rf = 0 \implies f = 0$.*

Proof. After taking the Fourier transform in y_n on both sides of (4.1), we have,

$$\widehat{Rf}(s, \mathbf{y}', \xi) = \sqrt{1+s^2} \int_0^\infty e^{-ist\xi} M\hat{f}_\xi(t, \mathbf{y}') \mathrm{d}t \tag{4.2}$$

where $\hat{f}_\xi$ is the Fourier transform in the x_n component evaluated at ξ. Let $s' = s\xi$. Then, for $\xi \neq 0$, we have

$$M\hat{f}_\xi(t, \mathbf{y}') = \frac{1}{2\pi} \int_{-\infty}^\infty \frac{\widehat{Rf}\left(\frac{s'}{\xi}, \mathbf{y}', \xi\right)}{\sqrt{1+\left(\frac{s'}{\xi}\right)^2}} e^{is't} \mathrm{d}s' \tag{4.3}$$

for all $t \geq 0$ and $\mathbf{y}' \in Q$. We have now established a link between cone transform (4.1) and the spherical Radon transform.

Let $Rf = 0$. Then, by (4.3), $M\hat{f}_\xi(t, \mathbf{y}') = 0$ for any $t \geq 0$, $\mathbf{y}' \in Q$, and $\xi \neq 0$. Furthermore, $\hat{f}_\xi$ is supported in Σ and its boundary, Q is convex and real-analytic. This, plus results of [15] on analytic regularity under the Bolker assumption, and the arguments in the proof of [20, Corollary 3.2] for the spherical transform show that, since $M\hat{f}_\xi = 0$ for all centers on Q, $\hat{f}_\xi = 0$, for any $\xi \neq 0$. As f is of compact support, the ξ component of $\hat{f}_\xi$, is an entire analytic function, and thus $\hat{f}_\xi = 0$ for all $\xi \in \mathbb{R}$. Therefore, $f = 0$, and this completes the proof. □

Discussion 4.2. The function, $\widehat{Rf}(s'/\xi, \mathbf{y}', \xi)/\sqrt{1+(s'/\xi)^2}$, is the Fourier transform of $M\hat{f}_\xi$ in the t variable at value s'. If f is compactly supported, then $M\hat{f}_\xi(t, \mathbf{y}')$ is a compactly supported function of t for any fixed $\mathbf{y}'$. Thus, the Fourier transform in t is an entire analytic function and, by analytic continuation, we need only the $s \in \Omega$, for some open $\Omega \subset \mathbb{R}$, to determine $\widehat{Rf}(s'/\xi, \mathbf{y}', \xi)/\sqrt{1+(s'/\xi)^2}$ everywhere. Therefore, we need only that $Rf(s, \mathbf{y}) = 0$ for $s \in \Omega$, and $\mathbf{y}' \in Q$, to show $f = 0$.

In cases when M has an explicit left inverse, M^{-1}, e.g., when Q is a sphere and S is cylinder, and we know Rf for all $s \in \mathbb{R}$, and $\mathbf{y} \in S$, then, using (4.3), we have the explicit expression for f in terms of Rf

$$f = \frac{1}{2\pi} \mathcal{F}_\xi^{-1} M^{-1} \left(\int_{-\infty}^\infty \frac{\widehat{Rf}\left(\frac{s'}{\xi}, \mathbf{y}', \xi\right)}{\sqrt{1+\left(\frac{s'}{\xi}\right)^2}} e^{is't} \mathrm{d}s' \right), \tag{4.4}$$

where $\mathcal{F}_\xi^{-1}$ is the inverse Fourier transform in the ξ variable.

In this section, we presented injectivity results for R_μ, and for R in the case when $h(s,x) = sx$. The above discussion provides an explicit inverse for the cone transform in the special case when M has an explicit left inverse. In the next section, we consider when h is an even function with a single maximum, as well as a generalisation of this case.

4.2. **Analytic inversion in the case of symmetric curves.** In this section, we provide a general inversion framework for surface of revolution Radon transforms where the surfaces have some symmetry. Throughout this section, we let

$$B_r^n(\mathbf{y}) = \{\mathbf{x} \in \mathbb{R}^n : |\mathbf{x} - \mathbf{y}| < r\}$$

denote the open unit ball in $\mathbb{R}^n$ of radius r. We will consider the same geometry as in section 3 but will reformulate the operator and add some hypotheses on the function h. Indeed, we suppose that $C = \{s > 0\}$ and for every s, $\Omega_{h,s} = \{x \ : \ (x,s) \in \Omega_h\}$ is a symmetric interval around the origin, that $h(s,\cdot)$ is an even function on this interval, that $h \to 0$ at the boundaries of this interval, that $h(s,\cdot)$ takes a single maximum at $x = 0$ where the second derivative h_{xx} does not vanish, that otherwise the h_x does not vanish, and that $h(s,0)$ is an increasing function with $h(s,0) \to 0$ as $s \to 0$. There are several examples of practical interest where h satisfies these hypotheses and we discuss them in section 5. In this case, equation 3.4 is equivalent to

$$Rf(s,\mathbf{y}) = \int_{\Omega_{h,s}} \int_{\Theta \in S^{n-2}} h(s,x)^{\frac{n-2}{2}} f(\sqrt{h}(s,x)\Theta + \mathbf{y}', y_n + x) \sqrt{1 + \frac{h_x^2}{4h}} \, \mathrm{d}S^{n-2} \mathrm{d}x \tag{4.5}$$

where $\mathrm{d}S^{n-2}$ is the surface measure on S^{n-2}. By the hypotheses on h, $\Omega_{h,s}$ can be split into two intervals $(-b(s), 0)$ and $(0, b(s))$, and $h(s,\cdot)$ is invertible on each of these intervals. In fact, because $h(s,\cdot)$ is even there will be a function $\mu(s,\cdot) : (0, h(s,0)) \to (0, b(s))$ such that

$$h(s, \mu(s,t)) = h(s, -\mu(s,t)) = t^2.$$

Then, changing coordinates $x = \pm\mu(s,t)$ in the inner integral of (4.5), we have

$$Rf(s,\mathbf{y}) = \sum_{k=0}^{1} \int_0^{\sqrt{h}(s,0)} \int_{\Theta \in S^{n-2}} t^{n-2} f\big(t\Theta + \mathbf{y}', (-1)^k \mu(s,t) + y_n\big) \sqrt{1 + \mu_t^2} \, \mathrm{d}S^{n-2} \mathrm{d}t.$$

By making a change of variables $\tilde{s} = \sqrt{h}(s,0)$, which is possible by the hypotheses, this becomes

$$Rf(\tilde{s},\mathbf{y}) = \sum_{k=0}^{1} \int_0^{\tilde{s}} \int_{\Theta \in S^{n-2}} t^{n-2} f\big(t\Theta + \mathbf{y}', (-1)^k \mu(s,t) + y_n\big) \sqrt{1 + \mu_t^2} \, \mathrm{d}S^{n-2} \mathrm{d}t. \tag{4.6}$$

We will show how to invert a transform slightly more general than (4.6) by first taking the Fourier transform in the y_n variable. Our generalisation is the following.

Let $\mu_j = \mu_j(s,t) \in C(\mathcal{T})$, for $1 \le j \le m$, be a set of functions which define m one-parameter families of curves, where $\mathcal{T} = \{(s,t) : a \le t \le s \le b\}$, for some $b > a \ge 0$. Then, we define the Radon transform

$$R_\mu f(s,\mathbf{y}) = \sum_{k=0}^{1} \sum_{j=1}^{m} \int_a^s g_j \int_{\Theta \in S^{n-2}} t^{n-2} f\left(t\Theta + \mathbf{y}', (-1)^k \mu_j(s,t) + y_n\right) \mathrm{d}S^{n-2} \mathrm{d}t, \tag{4.7}$$

where $g_j = g_j(s,t) = \sqrt{1 + \mu_{jt}^2}$, $\mu_{jt} = \frac{\mathrm{d}}{\mathrm{d}t}\mu_j$. The transform, R_μ, maps f to its integrals over the surfaces of revolution of symmetric continuous curves defined by the μ_j and is equal to R defined in section 3, as can be seen in (4.6), for the case when $m = 1$, $f = 0$ on $\cup_{\mathbf{s} \in S} B_a^n(\mathbf{s})$ (i.e., f is zero up to distance a from S), and h is even in x. For example, when $f = 0$ on $\cup_{\mathbf{s} \in S} B_a^n(\mathbf{s})$, $m = 1$ and $\mu_1(s,t) = \sqrt{s^2 - t^2}$, and $h(s,x) = s^2 - x^2$, then $R_\mu f = Rf$ defines the integrals of f over spheres, radii s with center $\mathbf{y} \in S$. The reason we introduce the μ_j in this section to define the surfaces of rotation, is for elegance and ease of calculation in the proofs of our main injectivity theorem (Theorem 4.3), presented later in this section. We take a sum of m integrals in (4.7) to keep the discussion more general. The $m = 1$ case is of the most practical interest, and later, in section 5, we discuss further examples of μ_j and h, and how they apply to CST, ECST, and URT.

Taking the Fourier transform in y_n on both sides of (4.7), yields

$$\begin{aligned}\widehat{R_\mu f}(s,\mathbf{y}',\xi) &= \int_a^s \sum_{j=1}^m g_j \cos(\xi\mu_j)\left[\int_{\Theta\in S^{n-2}} t^{n-2}\hat{f}_\xi\left(t\Theta+\mathbf{y}'\right)\mathrm{d}S^{n-2}\right]\mathrm{d}t \\ &= \int_a^s \tilde{K}_\xi(s,t) M\hat{f}_\xi(t,\mathbf{y}')\mathrm{d}t,\end{aligned} \tag{4.8}$$

where

$$\tilde{K}_\xi(s,t) = \sum_{j=1}^m g_j(s,t)\cos\left(\xi\mu_j(s,t)\right), \tag{4.9}$$

ξ is dual to x_n, $\hat{f}_\xi(\mathbf{x}') = \hat{f}(\mathbf{x}',\xi)$, and M is the spherical Radon transform introduced in section 4.1. Equation (4.8) is a Volterra equation of the first kind, which we aim to solve for $M\hat{f}_\xi$. Then we use known results on M [20, 15] to derive injectivity conditions on R_μ.

We now have our theorem, which provides injectivity conditions on R_μ.

Theorem 4.3. *Let $b > a \geq 0$, and let $\mathcal{T} = \{(s,t) : a \leq t \leq s \leq b\}$. Suppose that Q is the boundary of an open convex set $\Sigma \subset \mathbb{R}^{n-1}$. Let $f \in L^2_c(\Sigma\times\mathbb{R})$.*

Consider the conditions

(1) $f = 0$ at all points of distance less than a from S.
(2) μ_j is of the form $\mu_j(s,t) = \sqrt{s-t}\cdot\tau_j(s,t)$, where $\tau_j \in C^\infty(\mathcal{T})$, and $\tau_j(s,s) \neq 0$ for $s \in [a,b]$;
(3) S is a real-analytic manifold.

Under (2), (4.8) *is uniquely solvable. Under* (1), (2) *and* (3), $R_\mu f = 0$ *on* $[a,b]\times S$ *implies* $f = 0$ *at all points of distance less than b from S.*

Remark 4.4. Assumption (2) gives conditions on μ_j so that $M\hat{f}_\xi$ is uniquely recoverable from $R_\mu f$. For R in (4.6), this first assumption is satisfied because the second derivative h_{xx} does not vanish at $x = 0$. Assumption (3) provides injectivity conditions on M, as in [20, Theorem 2.4]. (2) and (3) combined give injectivity conditions for R_μ.

Remark 4.5. It is possible to prove an extension of Theorem 4.3 for operators without the symmetry condition (i.e. (4.7) without a sum in k) provided the μ_j satisfy certain asymptotic compatibility conditions at the boundary of their definition. However, this is not necessary for any of the practical examples given in section 5.

Proof of Theorem 4.3. Let us assume (2) holds. Given the specific form of the μ_j specified in (2), we have

$$\begin{aligned} g_j(s,t) &= \sqrt{1+\mu_{jt}^2} \\ &= \frac{\sqrt{(s-t)+\left((s-t)\tau_{jt}-\frac{1}{2}\tau_j\right)^2}}{\sqrt{s-t}} \\ &= \frac{\kappa_j(s,t)}{\sqrt{s-t}}.\end{aligned} \tag{4.10}$$

We have, $\kappa_j(s,s) = \frac{1}{2}|\tau_j(s,s)| > 0$ for $s \in [a,b]$, and $\kappa_j(s,t) > 0$, when $s \neq t$ and $(s,t) \in \mathcal{T}$. Therefore, since κ_j is continuous and $\mathcal{T}$ is compact, κ_j is bounded away from zero on $\mathcal{T}$ and $\kappa_j \in C^\infty(\mathcal{T})$.

Now, by (4.8), we have

$$\begin{aligned}\widehat{R_\mu f}(s,\mathbf{y}',\xi) &= \int_a^s \frac{\sum_{j=1}^m \kappa_j \cos(\xi\mu_j)}{\sqrt{s-t}} \left[\int_{\Theta\in S^{n-2}} t^{n-2}\hat{f}_\xi\left(t\Theta+\mathbf{y}'\right)\mathrm{d}S^{n-2}\right]\mathrm{d}t \\ &= \int_a^s \frac{K_\xi(s,t)}{\sqrt{s-t}} M\hat{f}_\xi(t,\mathbf{y}')\mathrm{d}t,\end{aligned} \tag{4.11}$$

where

$$K_\xi(s,t) = \sum_{j=1}^m \kappa_j(s,t)\cos\left(\xi\mu_j(s,t)\right). \tag{4.12}$$

We have

$$K_\xi(s,s) = \frac{1}{2}\sum_{j=1}^m |\tau_j(s,s)| > 0 \tag{4.13}$$

for $s\in[a,b]$, by (2), and

$$\begin{aligned}\frac{\mathrm{d}}{\mathrm{d}s}\cos(\xi\mu_j) &= -\xi\cdot\frac{(s-t)\tau_{js}-\tau_j}{\sqrt{s-t}}\sin(\xi\mu_j) \\ &= \phi_j\,\mathrm{sinc}(\xi\mu_j)\in C(\mathcal{T}),\end{aligned} \tag{4.14}$$

where $\phi_j = \xi^2\tau_j\left((s-t)\tau_{js}-\tau_j\right)\in C^\infty(\mathcal{T})$. Thus, $\frac{\mathrm{d}}{\mathrm{d}s}K_\xi\in C(\mathcal{T})$, given also the smoothness of the κ_j. Further, since $M\hat{f}_\xi\in L^2\left(\mathbb{R}_+\times\mathbb{R}^{n-1}\right)$, $\widehat{Rf}(s,\mathbf{y}',\xi)$ is an absolutely continuous function of s, by [19, Lemma 3.3]. Therefore, by [19, Theorems A and B], we can now solve the Volterra equation of the first kind (4.11) uniquely for $M\hat{f}_\xi(t,\mathbf{y}')$, for all $t\in[a,b]$, $\mathbf{y}'\in\mathbb{R}^{n-1}$, and $\xi\in\mathbb{R}$.

To finish the proof, let us assume $Rf=0$, and that (2) and (3) hold. Using the above calculations, $Rf=0$ implies $M\hat{f}_\xi(t,\mathbf{y}')=0$ for any $t\in[a,b]$, $\mathbf{y}'\in Q$, and $\xi\in\mathbb{R}$. As $\mathrm{supp}(f)$ is at least distance a from S, $M\hat{f}_\xi(t,\mathbf{y})=0$ for all $(t,\mathbf{y})\in[0,b)\times Q$ and $\hat{f}_\xi$ is supported in Σ. Since, in addition, Q is a convex real-analytic manifold by assumption (3), we can use the analytic regularity theorem in [15] under the Bolker assumption and the arguments in the proof of [20, Corollary 3.2] to show that $\hat{f}_\xi=0$ on $\cup_{\mathbf{y}'\in Q}B_b^{n-1}(\mathbf{y}')$, for any $\xi\in\mathbb{R}$. Therefore, $f=0$ on $\cup_{\mathbf{s}\in S}B_b^n(\mathbf{s})$. This completes the proof. □

Remark 4.6. Theorem 4.3 establishes a key link between R_μ and the spherical Radon transform, on which there exists a wealth of literature on the inversion properties. After taking the Fourier transform in y_n and inverting a 1-D Volterra operator in the first stages of the proof of Theorem 4.3, R_μ reduces to a spherical Radon transform, M, which is applied to slices in Fourier space, $\hat{f}_\xi$. In special cases, this connection to the spherical transform can be used to derive methods for inverting R_μ. For example, if $Q=S^{n-2}$ is a sphere and f is compactly supported on the interior of $S=Q\times\mathbb{R}$, then $\hat{f}_\xi$ is compactly supported on the interior of Q, for any $\xi\in\mathbb{R}$, and $\hat{f}_\xi$ can be recovered explicitly from $M\hat{f}_\xi$ using the formulae of [14].

5. Example applications

In this section, we give some example h and μ_j which have applications in CST, URT, and ECST. We only consider here the conditions on h and μ given in Theorem 3.2, and Theorem 4.3, respectively, which are needed in order for the Bolker condition and injectivity to hold. For the Bolker condition to hold in any of the examples given below, $\mathrm{supp}(f)$ must be bounded away from S, and S must also satisfy condition 2 of Theorem

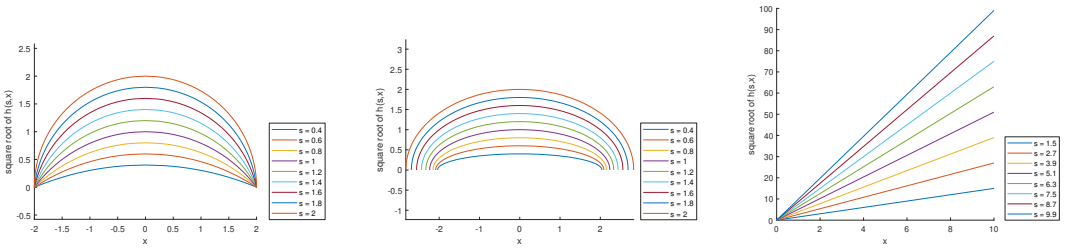

(A) circular arcs ($\alpha = 2$) (B) elliptic arcs ($c = 2$) (C) lines

FIGURE 2. Example $\sqrt{h}$ mappings which define circular and elliptic arcs, and straight line curves.

3.2. For injectivity to hold, we need $\text{supp}(f)$ to be bounded away from S, S to be real-analytic, and Q to be the boundary of a convex set, as specified in Theorem 4.3.

5.1. **Elliptic arcs with fixed linear eccentricity.** In this example, we consider the case when h defines an elliptic arc, and $\mathcal{R}(s, \mathbf{y})$ is an ellipsoid of revolution (or spheroid). Spheroid integral surfaces have applications in URT [31], and seismic imaging [7]. For example, in URT, the foci of the spheroids represent sound wave emitters and receivers, and the sound wave travel time determines the spheroid radii. We consider the special case when the foci of the spheroid are constrained to lie on S, and the linear eccentricity of the spheroid, c, is fixed. This case is of interest in the URT literature [1] as well.

Let

$$h(s,x) = \frac{s^2}{s^2+c^2}(s^2+c^2-x^2) \in C^\infty(\Omega_h), \tag{5.1}$$

where s is the minor ellipse radius, c is the fixed linear eccentricity, and $\Omega_h = \{(s,x) : s > 0, -\sqrt{s^2+c^2} < x < \sqrt{s^2+c^2}\}$. Then, for fixed $s > 0$, $x \to \sqrt{h}(s,x)$ defines an elliptic arc. See figure 2b, where we plot some example elliptic arc curves when $c = 2$.

We now aim to show that h satisfies the conditions of Theorem 3.2. First, it is clear that $h \to 0$ at the boundary of Ω_h. Also,

$$h_s(s,x) = \frac{s\left(c^4 - c^2(x^2-2s^2) + s^4\right)}{(s^2+c^2)^2}, \tag{5.2}$$

which is non-zero on Ω_h. Now, we have

$$\frac{h_x}{h_s} = -\frac{sx(s^2+c^2)}{c^4 - c^2(x^2-2s^2) + s^4}, \tag{5.3}$$

and it follows that

$$\frac{\mathrm{d}}{\mathrm{d}x}\left(\frac{h_x}{h_s}\right) = -s(s^2+c^2)\frac{c^4 + c^2(x^2+2s^2) + s^4}{\left(c^4 - c^2(x^2-2s^2) + s^4\right)^2}, \tag{5.4}$$

which is non-zero on Ω_h. Thus, the conditions of Theorem 3.2 are satisfied.

Let

$$\mu(s,t) = \sqrt{1 + \left(\frac{c}{s}\right)^2}\sqrt{s^2-t^2}.$$

Then, if h is defined as in (5.1), $f = 0$ on $\cup_{\mathbf{s}\in S} B_a^n(\mathbf{s})$, and $m = 1$, with $\mu_1 = \mu$, $Rf = R_\mu f$. We now aim to show the conditions on μ specified in Theorem 4.3 hold. We have $\mu(s,t) = \sqrt{s-t}\cdot\tau(s,t)$, where

$$\tau(s,t) = \sqrt{1 + \left(\frac{c}{s}\right)^2}\sqrt{s+t}.$$

Let $b > a > 0$. Then, τ is smooth on $\mathcal{T} = \{(s,t) : a \le s \le b, a \le t \le s\}$. Further,

$$\tau(s,s) = \sqrt{2}\sqrt{s}\sqrt{1 + \left(\frac{c}{s}\right)^2} \neq 0$$

for $s \in [a,b]$. Thus, the conditions of Theorem 4.3 are satisfied when $m = 1$, and $\mu_1 = \mu$.

5.2. **Circular arcs.** In this example, we consider the case when h defines a circular arc curve, and $\mathcal{R}(s,\mathbf{y})$ is the surface of revolution of a circular arc, which we call a lemon. A lemon is also the interior part of a spindle torus (see [22, figure 5]), which is a special kind of torus that self-intersects. Lemon integral surfaces have applications in CST [22]. A lemon self-intersects at two points, which we will call the "tips" of the lemon. In CST, the tips of the lemon represent source and detector positions, and the scattered photon energy determines the radius of the lemon. We consider the special case here where the distance between the tips of the lemon, α, is fixed.

Let

$$h(p,x) = \left(\sqrt{\alpha^2 + p^2 - x^2} - p\right)^2 \in C^\infty(\Omega_h), \tag{5.5}$$

where $\Omega_h = [0,\infty) \times (-\alpha, \alpha)$. Then, $x \to \sqrt{h}(p,x)$, for fixed $p \in [0,\infty)$, defines a circular arc. See figure 2a for an illustration of circular arc curves when $\alpha = 2$. In figure 2a, s relates to p via $s = \sqrt{\alpha^2 + p^2} - p$.

We now aim to show the conditions of Theorem 3.2 are satisfied. By (5.5), it is clear $h \to 0$ on the boundary of $\Omega_{h,p} = \{(p',x) \in \mathbb{R}^2 : p = p'\} \cap \Omega_h$, for any $p \in [0,\infty)$. We have,

$$h_p(p,x) = 2\left(\frac{p}{\sqrt{\alpha^2 + p^2 - x^2}} - 1\right)\left(\sqrt{\alpha^2 + p^2 - x^2} - p\right), \tag{5.6}$$

which is strictly less than zero on Ω_h. Now,

$$\frac{h_x}{h_p} = \frac{x}{\sqrt{\alpha^2 + p^2 - x^2} - p}, \tag{5.7}$$

and

$$\frac{\mathrm{d}}{\mathrm{d}x}\left(\frac{h_x}{h_p}\right) = \frac{(p^2 + \alpha^2) - p\sqrt{p^2 + \alpha^2 - x^2}}{\sqrt{p^2 + \alpha^2 - x^2}\left(\sqrt{p^2 + \alpha^2 - x^2} - p\right)^2}, \tag{5.8}$$

which is nonzero on Ω_h. To see this, note

$$\begin{aligned}(p^2 + \alpha^2) - p\sqrt{p^2 + \alpha^2 - x^2} &\ge (p^2 + \alpha^2) - p\sqrt{p^2 + \alpha^2} \\ &= \sqrt{p^2 + \alpha^2}\left(\sqrt{p^2 + \alpha^2} - p\right) > 0.\end{aligned} \tag{5.9}$$

Thus, the conditions of Theorem 3.2 are satisfied.

Let

$$\mu(s,t) = \sqrt{s - t}\sqrt{\frac{st + \alpha^2}{s}}.$$

Then, if h is defined as in (5.5) and $m = 1$, with $\mu_1 = \mu$, $Rf(p,\mathbf{y}) = R_\mu f\left(\sqrt{\alpha^2 + p^2} - p, \mathbf{y}\right)$, when $p \ge 0$. We will now show that μ satisfies the conditions of Theorem 4.3. We have, $\mu(s,t) = \sqrt{s - t} \cdot \tau(s,t)$, where

$$\tau(s,t) = \sqrt{\frac{st + \alpha^2}{s}}.$$

Let $b > a > 0$. Then, τ is smooth on $\mathcal{T} = \{(s,t) : a \leq s \leq b, a \leq t \leq s\}$. Further,

$$\tau(s,s) = s + \frac{\alpha^2}{s} > 0,$$

for $s \in [a,b]$. Thus, the conditions of Theorem 4.3 are satisfied when $m = 1$, and $\mu_1 = \mu$.

5.3. **Straight lines.** In this example, we consider the case when $h(s,x) = sx$ defines a straight line, gradient s, and $\mathcal{R}(s,\mathbf{y})$ is a cone. See figure 2c for some example straight line curves. Cone integral surfaces have applications in ECST and Compton camera imaging [29]. In CST, the vertex of the cone corresponds to a scattering location, and the scattered photon energy determines the gradient of the cone, s. In this case, the injectivity of R is covered in section 4.1. We aim to prove here that h satisfies the conditions of Theorem 3.2.

Let $h(s,x) = sx \in C^\infty(\Omega_h)$, where $\Omega_h = \mathbb{R} \times (0,\infty)$.Then, the set $\Omega_{h,s}$ in Theorem 3.2 assumption (1) is $\Omega_{h,s} = (0,\infty)$ and $h(s,\cdot) \to 0$ on the boundary of $\Omega_{h,s}$, which in this case is $\{0\}$. We have, $h_s(s,x) = x > 0$ on Ω_h. Further, $h_x/h_s = s/x$, and $\frac{\mathrm{d}}{\mathrm{d}x}(h_x/h_s) = -s/x^2 \neq 0$ on Ω_h. Thus, the conditions of Theorem 3.2 are satisfied.

6. Simulated image reconstructions

In this section, we present simulated three-dimensional image reconstructions from integrals over spheres, spheroids, and lemons, which were shown to satisfy the conditions of Theorem 3.2 and Theorem 4.3 in section 5. The surface of centers, S, we consider here is a cylinder. Throughout this section, $n = 3$, $Q = S^1$, and $S = Q \times \mathbb{R} = \{\mathbf{x} \in \mathbb{R}^3 : \sqrt{x_1^2 + x_2^2} = 1\}$. The target functions, f, we consider in this section have compact support which is contained within the interior of S, and which is bounded away from S, which is needed for the microlocal theory of Theorem 3.2, and the injectivity results of Theorem 4.3 to hold. S is also convex and real-analytic, which is in line with the conditions of Theorem 3.2 and Theorem 4.3. In all simulations conducted in the section, the conditions of Theorem 3.2 and Theorem 4.3 are satisfied.

6.1. **Data simulation.** The data is simulated using the exact model (4.7), with $m = 1$. The definition of μ_1 changes based on the integral surface, e.g., for spherical integrals we set $\mu_1(s,t) = \sqrt{s^2 - t^2}$. Let V_ξ be the Volterra operator of (4.8), and let $\mathcal{F}_3$ denote the partial Fourier transform in the x_3 variable. Then we simulate data as

$$R_\mu f = \mathcal{F}_3^{-1} V_\xi M \mathcal{F}_3 f, \tag{6.1}$$

where M is applied to each Fourier slice, $\hat{f}_\xi$, of f, as in (4.8). We simulate $R_\mu f(s,\mathbf{y})$ for $s \in [0.2, 2.2]$, and $\mathbf{y} = (\cos\theta, \sin\theta, y_3) \in S$, where $\theta \in [0, 2\pi]$, and $y_3 \in [-5,5]$. For spheres, s is the sphere radius. For spheroids, s is the minor radius, and we set the linear eccentricity, $c = 2$, as in figure 2b. For lemons, s is the height of the lemon, and we set the distance between the lemon tips, $\alpha = 2$, as in figure 2a. After the data is generated as in (6.1), we add Gaussian noise to $R_\mu f$ to simulate noise.

6.2. **Inversion methods.** We recover f from $R_\mu f$ by inverting the sequence of operators on the right-hand side of (6.1). Each operator is discretized and f is recovered on an $N \times N \times N$ pixel grid. Throughout this section, we set $N = 101$.

To apply and invert $\mathcal{F}_3$, we use the Fast Fourier Transform (FFT). To invert V_ξ, we use Tikhonov regularization, and the "backslash" function in Matlab. This is possible as each Volterra operator, V_ξ, is one-dimensional, and hence the discretized form is a small (in this case $N \times N$) matrix, which is stored in Matlab. We use the Landweber method, and Total Variation (TV) regularization methods to invert M. Specifically, to implement

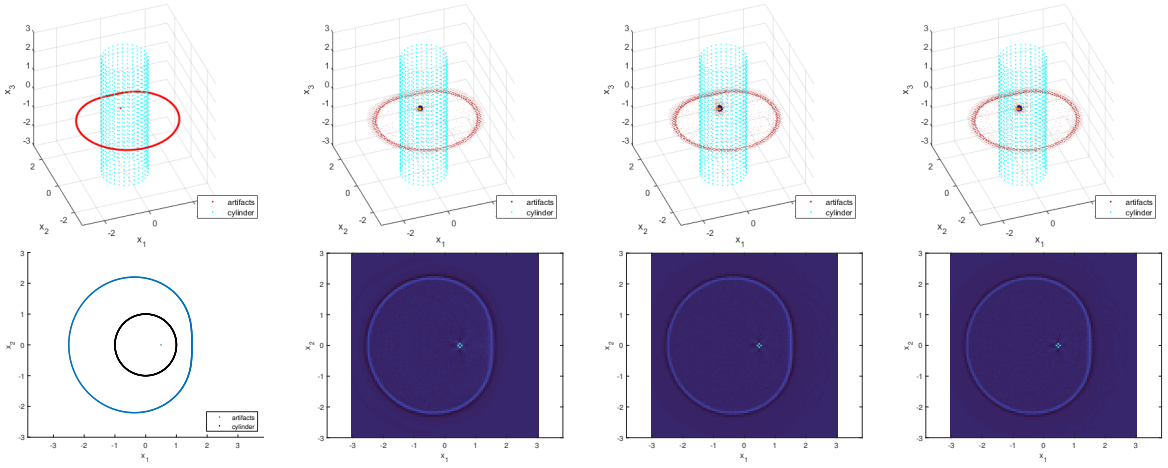

predicted sphere spheroid lemon

FIGURE 3. Predicted and observed artifacts due to Bolker for a variety of integral surfaces of revolution with centers on a cylinder. Top row - 3-D view. Bottom row - (x_1, x_2) plane cross-sections. 1% Gaussian noise was added in this example.

TV, we use the Conjugate Gradient Least Squares (CGLS) method in combination with TV denoising. The Landweber method enforces relatively weak regularization, and is included mainly to highlight some of the artifacts we would expect to see as predicted by Theorem 3.2. The CGLS-TV method is included to show the effects of a more powerful regularizer.

6.3. **Delta function reconstructions.** In this section, we present reconstructions of a delta function, δ, which is located on the interior of S. By theorem 3.2, when we recover δ from its integrals over spheres, lemons, or spheroids, with centers on S, we would expect to see artifacts which are the reflections of δ in planes tangent to S. Given the convexity of S in this case, and as δ is supported on the interior of S, the artifacts due to Bolker should also be constrained to the exterior of S. In figure 3, we show reconstructions of an example δ when using the Landweber method to invert M, as described in section 6.2. On the left-hand of figure 3, we show the artifacts due to Bolker as predicted by Theorem 3.2. In the reconstructions, the delta function is reflected in every plane tangent to S, which forms a cardioid type curve which is embedded in the (x_1, x_2) plane. This is as predicted by our theory, and the predicted and observed artifact curves match exactly.

6.4. **Phantom reconstructions.** In this sub-section, we present simulated reconstructions of an image phantom. The phantom we consider is a hollow cuboid as pictured in the left-hand column of figure 6. In figure 4, we show the size of the hollow cube phantom, and how it fits inside of S. We also show example curves which define the surfaces of revolution, in the case of spheres, spheroids, and lemons.

In figure 5, we show example $R_\mu f$ sinograms for sphere, spheroid, and lemon integral surfaces, where $R_\mu f$ is generated as specified in sub-section 6.1. The edges of the hollow cuboid phantom can be seen in the $\{\theta = 0\}$ plane cross-sections, although they are smoothed out due to the application of R_μ. In the $\{y_3 = 0\}$ plane and $\{s = 1.2\}$ plane cross-sections, the sinograms are $\pi/2$ periodic as a function of θ. This is due to the four-fold rotational symmetry of the hollow cuboid about the x_3 axis.

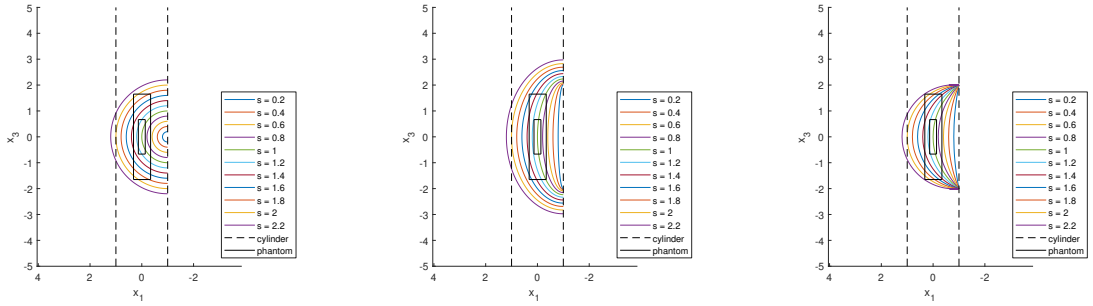

(A) spheres (B) spheroids (C) lemons

FIGURE 4. Hollow cube phantom and example curves which form the surfaces of revolution in the case of spheres, spheroids, and lemons. The μ_j and h functions which define the curves shown are provided in section 5. The sphere case in (A) is a special case of a spheroid, when $c = 0$, where c is the linear eccentricity, as defined in sub-section 5.1.

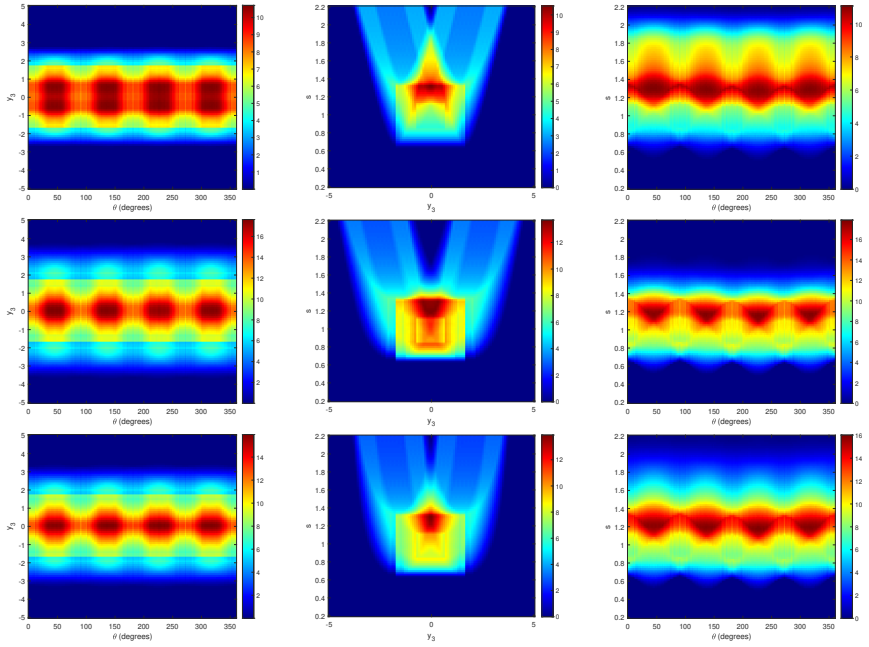

$\{s = 1.2\}$ plane $\{\theta = 0\}$ plane $\{y_3 = 0\}$ plane

FIGURE 5. Example $R_\mu f$ sinograms when f is a hollow cuboid. Sinograms are generated for three integral surfaces, namely spheres (top row), spheroids (middle row), and lemons (bottom row). We show three cross-sections for each integrals surface, which are specified in the sub-figure caption.

See figure 6, where we have presented reconstructions of the hollow cube phantom from the sinogram data in figure 5, with 5% added Gaussian noise, and see figure 7a where we plot the relative least-squares reconstruction errors for varying levels of added Gaussian noise. The Tikhonov and TV smoothing parameters used for each noise level are given on the x axis of figure 7a. To reconstruct the hollow cube phantom, we implemented the GCLS-TV algorithm as described in sub-section 6.2. The spheroid data reconstructions appear sharpest overall, when compared to the sphere and lemon reconstructions, and

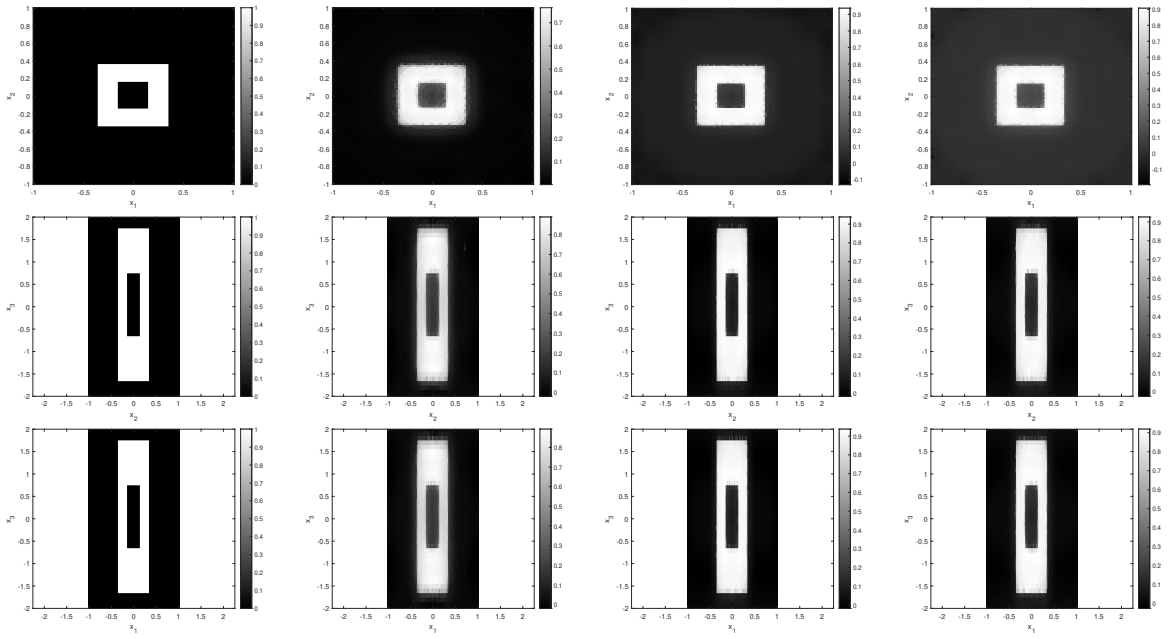

ground truth spheres spheroids lemons

FIGURE 6. Reconstructions of hollow cuboid with 5% added Gaussian noise. Top row - (x_1, x_2) plane. Middle row - (x_2, x_3) plane. Bottom row - (x_1, x_3) plane.

this is particularly noticeable in the (x_2, x_3) and (x_1, x_3) cross-sections. The sphere reconstructions are the most blurred, and offer the lowest image quality. This is verified by the reconstruction error plots in figure 7a, as the sphere integral reconstructions are shown to have the greatest error, when compared to lemon and spheroid integrals, and the spheroid reconstructions have the least error, particularly at higher noise levels (i.e., when the added noise is greater than or equal to 5%).

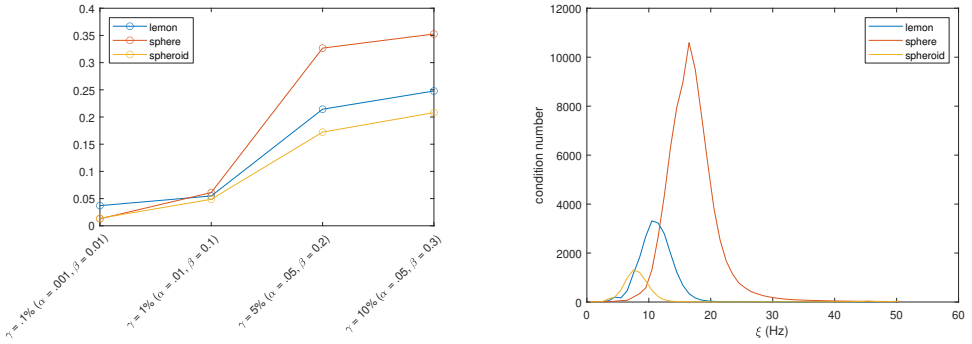

(A) least-squares errors (B) condition numbers

FIGURE 7. (A) - least-squares error curves for varying noise levels (γ), corresponding to each integral surface considered. The Tikhonov and TV smoothing parameters, α and β, respectively, corresponding to each γ, are given on the x axis in (A). (B) - condition number plots of the V_ξ operators, for varying ξ values, and for different integral surfaces of revolution.

The sphere, spheroid, and lemon surfaces are defined using different μ_1, which changes the V_ξ operators in (6.1). The remaining operations in (6.1), e.g., M, remain constant,

and do not vary with the integral surface. Thus, the differences in stability of inversion of R_μ, for different integral surfaces, can be quantified through analysis of the V_ξ. To investigate this, we plot the condition numbers of the V_ξ for varying ξ, and for sphere, spheroid, and lemon integral surfaces. See figure 7b. The largest peak in condition number occurs in the sphere curve, and the area under the sphere condition number curve is the largest. The spheroid condition numbers have the smallest peak, and area under the curve. Thus, the V_ξ operators exhibit the greatest inversion instability in the sphere case, when compared to spheroids or lemons, which corresponds to greater noise amplification in the image reconstructions, and this is verified by figure 7a. More generally, we notice that the area under the condition number curve correlates positively with the area under the error curves in figure 7a, which is to be expected as the condition number bounds the least squares error. This suggests that, in certain geometries (such as considered here), reconstructing f from spheroid data is preferred when compared to sphere data, in terms of inversion stability. This could have important implications in an application such as URT. In URT, the foci of the spheroid correspond to sound wave emitters and receivers. When the linear eccentricity, $c = 0$, the spheroids reduce to spheres, and the sound waves are emitted and received at the same point. In this example, setting $c = 2$ has advantages over the $c = 0$ case in terms of inversion stability. This has implications regarding scanner design in URT, e.g., we could compare the area under the condition number curves for a range of c to determine the optimal c, which, in the context of URT, is the distance between the emitter and receiver. This is an idea which warrants further investigation, which we aim to address in future work.

7. Conclusion

In this paper, we presented microlocal and injectivity analyses of a novel Radon transform, R, which defines the integrals of a function, f, over surfaces of revolution with centers on generalized surfaces $S = Q \times \mathbb{R}$ in $\mathbb{R}^n$, where $Q \subset \mathbb{R}^{n-2}$ is a smooth embedded hypersurface. In Theorem 3.2, we analyzed R as an FIO, and provided conditions on h and S which are necessary and sufficient for the Bolker condition to hold. The conditions on h involve the first and second order derivatives of h, which can be calculated and verified simply for many examples of interest, e.g., in URT, when h defines a semicircle or elliptic arc. The conditions on S are geometric and require checking if planes tangent to S intersect the support of f. In section 4, the surface of revolution transforms were shown to be closely related to the spherical Radon transform, and, using this idea, we proved injectivity results in Theorem 4.3.

In section 6, we presented condition number plots of the Volterra operators, V_ξ, which were used in the proof of Theorem 4.3. The area under the condition number curve was shown to correlate positively with the least-squares reconstruction error. Interestingly, the condition number plots had an approximate bell shape, and peaked at intermediate frequency values, ξ. In further work, we aim to investigate in more detail how the location and size of the condition number peak relates to the Volterra operators in (4.8), and if we can predict the peak location and magnitude analytically.

Acknowledgements:

The first author wishes to acknowledge funding support from Brigham Ovarian Cancer Research Fund, The V Foundation, Abcam Inc., and Aspira Women's Health. Sean Holman was supported by the Engineering and Physical Sciences Research Council (EPSRC) grant number EP/V007742/1. The third author's research was partially supported by Simons grant 708556. The authors would like to thank the Isaac Newton Institute for

Mathematical Sciences, Cambridge, for support and hospitality during the programme Rich and Nonlinear Tomography where work on this paper was undertaken. This programme was supported by EPSRC grant number EP/R014604/1.

References

[1] G. Ambartsoumian, J. Boman, V. P. Krishnan, and E. T. Quinto. Microlocal analysis of an ultrasound transform with circular source and receiver trajectories. In *Geometric analysis and integral geometry*, volume 598 of *Contemp. Math.*, pages 45–58. Amer. Math. Soc., Providence, RI, 2013.

[2] L.-E. Andersson. On the determination of a function from spherical averages. *SIAM Journal on Mathematical Analysis*, 19(1):214–232, 1988.

[3] P. Caday. Cancellation of singularities for synthetic aperture radar. *Inverse Problems*, 31(1):015002, 22, 2015.

[4] J. Cebeiro, C. Tarpau, M. A. Morvidone, D. Rubio, and M. K. Nguyen. On a three-dimensional compton scattering tomography system with fixed source. *Inverse Problems*, 37(5):054001, 2021.

[5] J. J. Duistermaat and L. Hormander. *Fourier integral operators*, volume 2. Springer, 1996.

[6] R. Gouia-Zarrad and G. Ambartsoumian. Exact inversion of the conical Radon transform with a fixed opening angle. *Inverse Problems*, 30(4):045007, 12, 2014.

[7] C. Grathwohl, P. C. Kunstmann, E. T. Quinto, and A. Rieder. Imaging with the elliptic radon transform in three dimensions from an analytical and numerical perspective. *SIAM Journal on Imaging Sciences*, 13(4):2250–2280, 2020.

[8] V. Guillemin and S. Sternberg. *Geometric Asymptotics*. American Mathematical Society, Providence, RI, 1977.

[9] M. Haltmeier and S. Moon. The spherical radon transform with centers on cylindrical surfaces. *Journal of Mathematical Analysis and Applications*, 448(1):567–579, 2017.

[10] L. Hörmander. Fourier Integral Operators, I. *Acta Mathematica*, 127:79–183, 1971.

[11] L. Hörmander. *The analysis of linear partial differential operators. I.* Classics in Mathematics. Springer-Verlag, Berlin, 2003. Distribution theory and Fourier analysis, Reprint of the second (1990) edition [Springer, Berlin].

[12] L. Hörmander. *The analysis of linear partial differential operators. III.* Classics in Mathematics. Springer, Berlin, 2007. Pseudo-differential operators, Reprint of the 1994 edition.

[13] L. Hörmander. *The analysis of linear partial differential operators. IV*. Classics in Mathematics. Springer-Verlag, Berlin, 2009. Fourier integral operators, Reprint of the 1994 edition.

[14] L. A. Kunyansky. Explicit inversion formulae for the spherical mean radon transform. *Inverse problems*, 23(1):373, 2007.

[15] M. Mazzucchelli, M. Salo, and L. Tzou. A general support theorem for analytic double fibration transforms. *arXiv:2306.05906V1 [math.AP]*, 6 2023.

[16] L. V. Nguyen and T. A. Pham. Microlocal analysis for spherical Radon transform: two nonstandard problems. *Inverse Problems*, 35(7):074001, 15, 2019.

[17] V. P. Palamodov. A uniform reconstruction formula in integral geometry. *Inverse Problems*, 28(6):065014, 2012.

[18] E. T. Quinto. The dependence of the generalized Radon transform on defining measures. *Trans. Amer. Math. Soc.*, 257:331–346, 1980.

[19] E. T. Quinto. The invertibility of rotation invariant Radon transforms. *J. Math. Anal. Appl.*, 94:602–603, 1983.

[20] E. T. Quinto. Support Theorems for the Spherical Radon Transform on Manifolds. *International Mathematics Research Notices*, 2006:1–17, 2006. Article ID = 67205.

[21] G. Rigaud. 3d compton scattering imaging with multiple scattering: Analysis by fio and contour reconstruction. *Inverse Problems*, 2021.

[22] G. Rigaud and B. N. Hahn. 3D Compton scattering imaging and contour reconstruction for a class of Radon transforms. *Inverse Problems*, 34(7):075004, 2018.

[23] B. Rubin. Inversion formulas for the spherical radon transform and the generalized cosine transform. *Advances in Applied Mathematics*, 29(3):471–497, 2002.

[24] B. Rubin. A note on the sonar transform and related Radon transforms. *arXiv:2206.05854 [math.FA]*, page 13, 2022.

[25] W. Rudin. *Functional analysis*. McGraw-Hill Book Co., New York, 1973. McGraw-Hill Series in Higher Mathematics.

[26] P. Stefanov and G. Uhlmann. Is a curved flight path in SAR better than a straight one? *SIAM J. Appl. Math.*, 73(4):1596–1612, 2013.
[27] F. Terzioglu. Some analytic properties of the cone transform. *Inverse Problems*, 35(3):034002, 2019.
[28] F. Terzioglu. Recovering a function from its integrals over conical surfaces through relations with the radon transform. *Inverse Problems*, 39(2):024005, 2023.
[29] F. Terzioglu, P. Kuchment, and L. Kunyansky. Compton camera imaging and the cone transform: a brief overview. *Inverse Problems*, 34(5):054002, 16, 2018.
[30] F. G. Tricomi. *Integral equations*. Dover Publications, Inc., New York, 1985. Reprint of the 1957 original.
[31] J. Webber, S. Holman, and E. T. Quinto. Ellipsoidal and hyperbolic Radon transforms; microlocal properties and injectivity. *Journal of Functional Analysis*, 285:110056, 2023. arXiv:2212.00243 [math.FA].
[32] J. W. Webber. On a cylindrical scanning modality in three-dimensional compton scatter tomography. *arXiv preprint arXiv:2307.03896*, 2023.
[33] J. W. Webber and E. L. Miller. Bragg scattering tomography. *Inverse Problems and Imaging*, 15(4):683–721, 2021.
[34] J. W. Webber and E. T. Quinto. Microlocal analysis of generalized radon transforms from scattering tomography. *SIAM Journal on Imaging Sciences*, 14(3):976–1003, 2021.